Official journal of the JHL 2689-9620
www.light-am.com

Letter to the Editor Open Access

Additive Manufacturing Fiber Preforms for Structured Silica Fibers with Bismuth and Erbium Dopants

Yushi Chu[1,2,3,4], Xinghu Fu[1,5], Yanhua Luo[1], John Canning[2], Jiaying Wang[1], Jing Ren[3], Jianzhong Zhang[3,*] and Gang-Ding Peng[1,*]

Dear Editor

Silica optical fibers have attracted a lot of attention because they are widely used in communications and sensing, and forming today's internet backbone. Driving much of the Internet-of-Things (IoT) evolution, optical fibers are expanding from a single function transmission technology to perform multiple functions and a growing need for various custom-design application-specific optical fibers. Current optical fiber manufacturing based on chemical vapor deposition (CVD) technologies together with stack-and-draw approaches used for structured optical fibers faces numerous challenges in enabling more complex geometries multimaterial composite fibers and multicore fibers. The additive manufacturing, or 3D printing, offers a solution to address all those challenges, and may potentially disrupt the optical fibers fabrication and bring in an evolution to IoT[1–2].

The additive manufacture of optical fiber preforms and optical fiber has recently been proposed and demonstrated[3–6]. A key challenge of 3D printing-based silica optical fibers is the high processing temperatures of silica glass that conventional top down approaches demand. For this reason, we exploited and extended recent reports of small-scale glass "bulk or slice" printing[7–15] beyond a few millimeters to centimeters[16] to demonstrate it was possible to additively manufacture optical fibers. Further, various active dopants were introduced. These include oxides and ions of bismuth and erbium to create additively manufactured bismuth and erbium co-doped optical fiber (BEDF). These fibers are known to have an ultra-broadband near infrared (NIR) luminescence covering the whole telecommunications O-L bands with 830 nm pump excitation, potentially appearing to be a promising active medium of fiber amplifiers for the next generation of fiber communication system[17–23].

In this letter, we report BEDFs with one and seven cores drawn from 3D printed preforms. The capability of 3D printing technology to produce complex and arbitrary fiber structures was demonstrated without the necessary time-consuming separation and integration processes involved in the traditional preform manufacture. In addition, a range of dopants, namely Bi^{3+}, Er^{3+}, Ge^{4+}, Ti^{4+} and Al^{3+} are introduced, further proving its diverse materials manufacturing capability. Care is needed in adjusting drawing conditions and method as the number of cores increases, leading to effective lower melting points in the preform.

As reported in ref. 16, the fabrication of 3D printed preforms involved five steps: (1) preparing UV sensitive resin embedded with amorphous silica nanoparticles; (2) printing designed preform utilizing a commercial DLP 3D printer; (3) filling the prepared resin into the holes of the

Correspondence: Jianzhong Zhang (zhangjianzhong@hrbeu.edu.cn) or Gang-Ding Peng (g.peng@unsw.edu.au)
[1]Photonics and Optical Communications, School of Electrical Engineering and Telecommunications, University of New South Wales, Sydney, NSW 2052, Australia
[2]interdisciplinary Photonics Laboratories, University of Technology Sydney, NSW 2007 & University of Sydney, NSW 2006 Australia
Full list of author information is available at the end of the article.

printed cladding preform followed by thermal-polymerization; (4) debinding and pre-sintering process driven by annealing to remove moisture and polymer support and pre-fusing of nanoparticles; and (5) higher temperature sintering to further remove impurities and fuse silica nanoparticles into glass during fiber drawing. The fiber preforms with structures of one and seven cores shown in the first row of Fig. 1e were first designed using AutoCAD. The inner d and outer D diameters of the fiber preforms are d = 3 mm and D = 22 mm, respectively. The distance between two closest cores Λ is 5 mm and the preform length L is 40 mm. The designed preforms were then loaded into a 3D direct light projection (DLP) printer (Asiga Australia: model PRO2). The preforms were printed 2D layer-by layer using near UV light (λ = 385 nm) translated in the vertical direction. The main printing parameters are UV light intensity I_{UV}, UV curing time t_{curing} and layer thickness τ, which are I_{UV} = 5.8 mW/cm^2, t_{curing} = 3.5 s, and τ = 75 μm, respectively.

The composition of the resin used for preform fabrication is described in the Method section. The fabricated preforms were annealed to remove moisture and then sintered to debind the polymer resin using a high temperature furnace (Furnace Technologies Australia, 1700 M). The preforms were heated up to T = 150, 300, 600, 800 and 1200 ℃ for 2, 4, 4, 1.5 and 2 hrs, with the heating rate of 0.5 ℃ /min and 3 ℃ /min, respectively, before and after T = 600 ℃. The mass, diameter and height changes of the fiber preforms were also investigated during the debinding process as demonstrated by the inset of Fig. 1b. The mass of the preforms decreases when the debinding temperature is under T < 600 ℃, and then is unchanged in the following process. This is consistent with removal of the polymer and other impurities at T < 600 ℃. When annealed at higher temperatures (T > 600 ℃) the preforms begin to shrink, the shrinkage of preform diameters and heights were around 28% and 27% respectively from T = 600 ℃ to 1200 ℃, as shown in the inset of Fig. 1b. If the preform were completely sintered to the dense glass state, the theoretical shrinkage would be 34%[24–25]. The temperature process of 600−1200 ℃ in this experiment was only to densify the fiber preform and improved its mechanical strength for the next step of fiber drawing, rather than sintering the preform into a glass, therefore the shrinkage was smaller than the theoretical value.

The preform after debinding was inserted into a Heraeus F300 quartz tube and drawn into the fiber using a commercial fiber drawing tower. The temperature during the whole fiber drawing process was logged during drawing shown in Fig. 1c. Similar to the previous work[16], the drawing temperature and pressure are kept to T = 1850 ℃ and P = 50 mbar, respectively. The fiber preform was heated to T = 810 ℃, and kept for 3 hrs at a pressure of P = 50 mbar for removing the moisture absorbed by the preform due to the porous structure during storage. The inserted X-ray diffraction (XRD) pattern was obtained by using the powdered 3D-printed BEDF without coating.

An optical assessment was carried out of the cores of the BEDFs. The cross-section microscopy images of two kinds

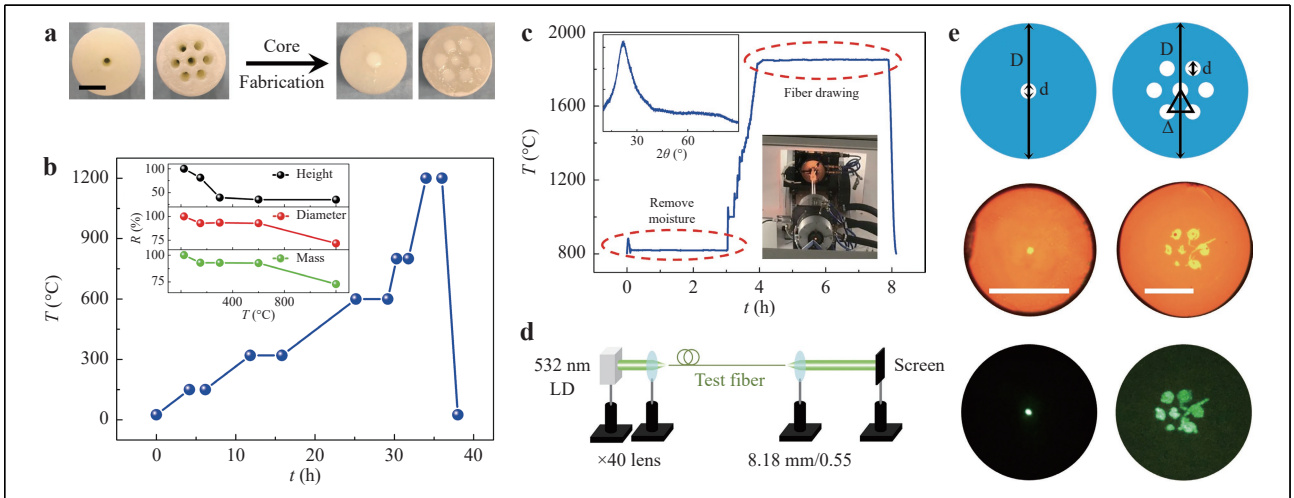

Fig. 1 **a** Images of the 3D printed preforms (left) and subsequently filled cores (right), the scale bar is 10 mm; **b** Temperature setting of the preform debinding process. Inset is the remaining ratio of mass and size during the debinding process; **c** Temperature change of the fiber drawing process. Insets are the XRD pattern of the drawn fiber and the photo of the drawing tower; **d** Experimental setup for transmission pattern measurement with a 532 nm laser diode (LD); **e** Designed preform structures (first row), fiber cross-section images recorded by a microscope with 50 μm scale bar (second row) and the transmission output pattern of the BEDFs projected onto a screen (third row).

of BEDFs are shown in the middle row of Fig. 1e. In all cases the core is not perfectly circular. As for the seven cores BEDFs, although multicore structures are kept, crack and shrinkage are noticed. It appears that the cores have physically displaced, reflecting a poor fit of the preform with the Heraeus tube and a too high fiber drawing temperature. To determine the element distribution of the fiber core and cladding after the high-temperature drawing, electron probe micro-Analysis (EPMA) was performed on the 7-core cross section shown in Fig. 2a. The Ge and Ti distributions are in the core whereas the Si is located as expected in both the core and cladding areas, shown in Fig. 2b–d. The Bi and Er were not detected because the concentrations were too low. A hole is presented in one of the cores which arises owing to the air bubbles entrapped during the fiber drawing and may be eliminated via the optimization of the fabrication process.

The three-dimensional refractive index of BEDFs was further measured with a SHR-1802 optical fiber index analyzer. The refractive index difference between core and cladding is obvious in the seven cores BEDFs, despite the existence of the melted state of the core and cladding due to excessive temperature during the fiber drawing process, shown in Fig. 3b. The maximum refractive index difference between the core and the cladding is $\Delta n \sim 0.01$ in the single core BEDF, demonstrated in Fig. 3a. The cut-off wavelength was estimated to be $\lambda_c \sim 800$ nm for the single core BEDF with the core diameter of $d \sim 3.5$ μm as shown in Fig. 3a, where the measured cutoff was located at $\lambda \sim 757$ nm. The value is smaller than the target one ($\lambda_c \sim 1000$ nm) based on material concentrations because of material evaporation during the fabrication process, a quantity that can be taken into account in subsequent pulls.

In addition, the fiber loss was measured by the cutback over the wavelength range of λ = 750−1600 nm, the experimental configuration and the loss spectrum of the single core BEDF are shown in Fig. 4a, b. Four absorption peaks are clearly observed. The absorption at λ = 810 nm is attributed to a third water overtone and possibly a bismuth active center related to a speculative Si (BAC-Si)[23]. At λ = 1535 nm the absorption is due to Er^{3+}[26]. However, the absorption peak of Er^{3+} is not particularly significant because of the relatively low doping concentration. Another absorption peak at λ = 980 nm is characteristic of a second overtone band of water ~ 1 um and may have a component from a center related to Al (BAC-Al) [23] and Er^{3+}[26]. The similar situation occurs at the absorption peak at λ = 1380 nm, for which the absorption of BAC-Si overlaps with the first OH overtone is responsible. It is worth noting that the absorption at λ = 1380 nm is $\alpha \sim 12.7$ dB/m, an improvement over previous results for a germanosilicate fiber ($\alpha \sim 20.9$ dB/m at 1380 nm)[16] where moisture and background scattering due to core asymmetry gives rise to an additional loss of ~ 8.0 dB/m. It's worth noting that the optical fiber in this report was doped with bismuth compared to the dopants-free optical fiber in Ref. 16, to be precise, the loss difference was at least 8 dB/m because of losses related with the doping of bismuth. This reduction is simply the removal of that component with an additional annealing at 810 ℃ during the fiber drawing process[27]. The losses of three cores in the seven cores BEDF were individually tested at 632.8 nm using a He-Ne laser, labeled with yellow font in the Fig. 4b. The single core fiber has a smaller loss, while the multicore fibers have greater losses partly because the presence coupling between the cores. Besides, some of the cores are so asymmetric that they have turned into a tubular shape, resulting in nontrivial scattering from both the inside and outside of the cores. This is direct evidence of flowing and the drawing temperature being well above the melting temperature of the preform.

The luminescent spectra obtained by pumping at λ = 830 nm and 980 nm were recorded with a monochromator and a photodetector, as shown in Fig. 4c. A lock-in amplifier was used to boost the signal to noise ratio. For the λ = 830 nm excitation, there are three luminescence bands over λ = (1000−1600) nm - see Fig. 4d. The first two peaks are located at λ = 1100 nm and λ = 1420 nm with bandwidths of $\Delta\lambda_{FWHM}$ = 150 nm and $\Delta\lambda_{FWHM}$ = 100 nm, attributed to the BAC-Al and BAC-Si respectively[17,23]. The

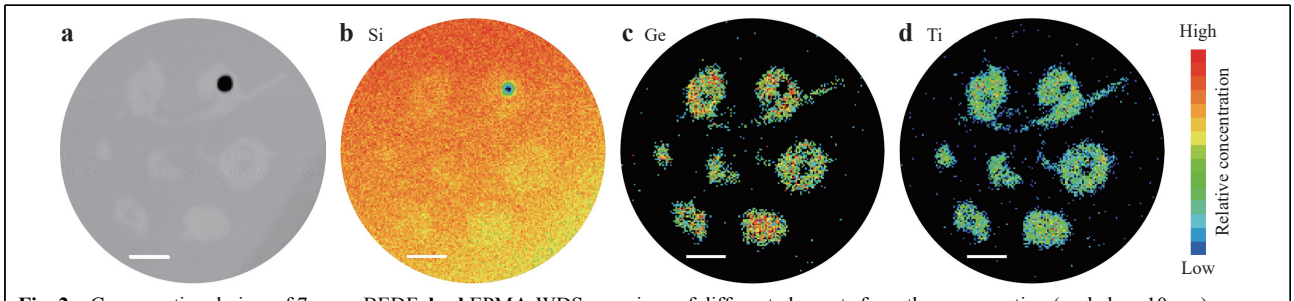

Fig. 2 a Cross-sectional view of 7 cores BEDF, **b**–**d** EPMA-WDS mappings of different elements from the cross section (scale bar: 10 μm).

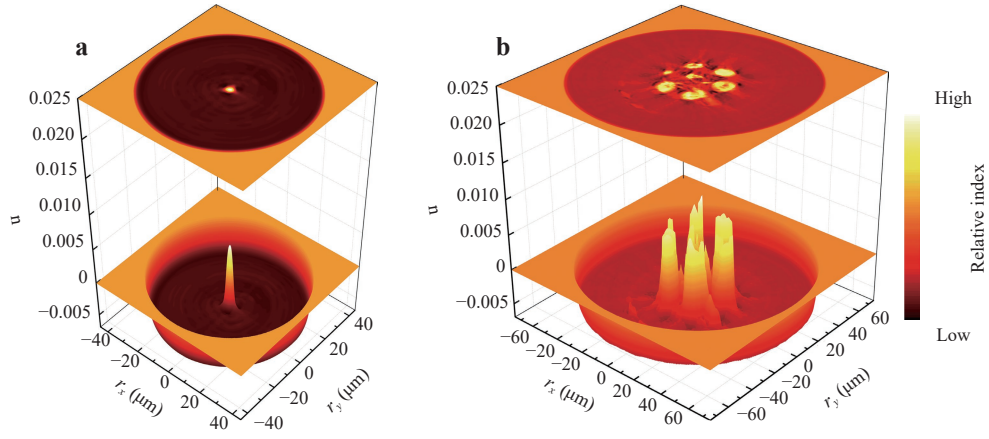

Fig. 3 Three-dimensional refractive index profiles of **a** single and **b** seven cores BEDF.

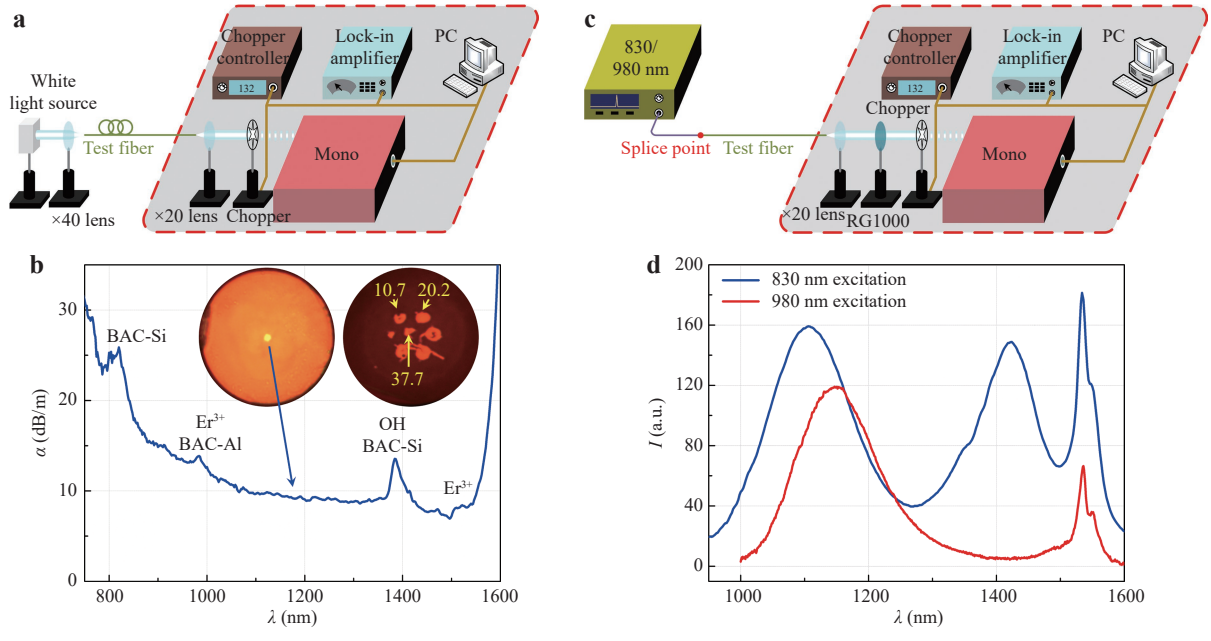

Fig. 4 a Experimental configuration of loss measurement by the cut-back method; **b** loss spectrum of the 3D printed single core and seven cores BEDFs; **c** experimental configuration of the emission measurement of a single core BEDF; **d** emission spectra of a single core BEDF excited by the 830 nm and 980 nm lasers.

λ = 1535 nm peak with $\Delta\lambda_{FWHM}$ = 32 nm is attributed to the Er^{3+}: $^4I_{13/2} \rightarrow {}^4I_{15/2}$ transition. Similarly, two peaks at λ = 1150 nm $\Delta\lambda_{FWHM}$ = 148 nm and λ = 1535 nm with $\Delta\lambda_{FWHM}$ = 28 nm under the λ = 980 nm pumping are attributed to the BAC-Al and Er^{3+} emissions, respectively. The wider FWHM and the peak shift with different excitations of BACs show typical unshielded *d-d* transitions of bismuth ions. The mode of single core BEDF was analyzed at the emission peaks where λ = 1100, 1420 and 1530 nm. Only LP_{01} mode exists, and the mode distributions are demonstrated in Fig. 5a–c. The mode fields are still elliptical as determined by the shape of the fiber core. The long/short axis of the mode field diameters are 5.2/ 5.0, 6.9/ 6.6 and 7.6/ 7.4 μm at 1100, 1420 and 1530 nm, respectively.

In summary, bismuth and erbium co-doped optical fibers with single- and seven-cores were drawn from 3D printed preforms. We show that the asymmetry arises principally from too high temperature and melting of the core and cladding of the preform within the Heraeus silica tube. The broadband NIR luminescence is obtained under the 830 nm and 980 nm excitations. The fiber loss in the single core fiber is substantially reduced as compared to the previous reports most likely due to a) the removal of water via the

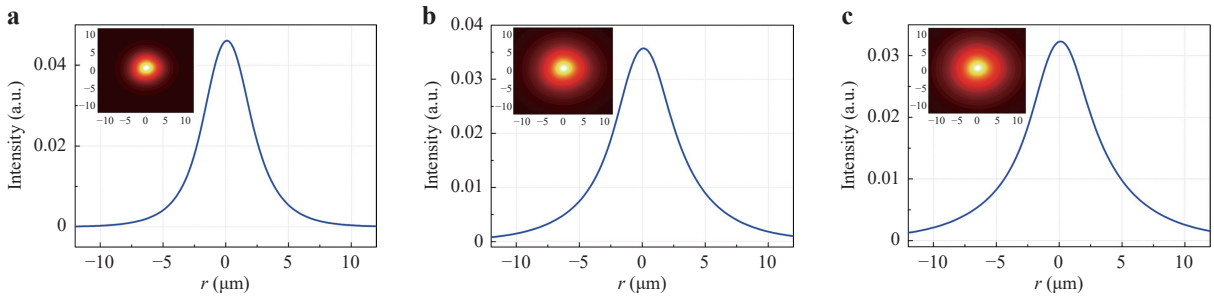

Fig. 5 Mode analysis at **a** 1100, **b** 1420 and **c** 1530 nm of the single core BEDF.

additional annealing and sintering treatment, and b) the improved symmetry due to the better shape match between the preform and the Heraeus tube. 3D printing technology promises to revolutionize specialty optical fibers permitting new functionalities. For example, it can easily realize multicore fiber fan-in/fan-out or ideal mode coupling in space division multiplexing without any splicing.

Methods

Materials

2-hydroxyethyl methacrylate (HEMA), 2-phenoxyethanol (POE), tetra(ethylenglycol) diacrylate (TEGDA), diphenyl(2,4,6- trimethylbenzoyl) phosphine oxide (DPO), hydroquinone, GeO_2, TiO_2, $Bi_2(Al_2O_4)_3$, $ErCl_3$ and 2,2-azobis(2-methylpropionitrile) (AIBN) were purchased from Sigma-Aldrich Australia. Amorphous SiO_2 nanoparticles with a mean diameter of 40 nm was bought from Evonik Australia labeled as Aerosil OX50.

Fabrication of BEDF preforms

For the fiber cladding, 37.39% amorphous SiO_2 nanoparticles, 36.91 wt% HEMA, 19.04 wt% POE, 6.35 wt% TEGDA, 0.20 wt% DPO and 0.10 wt% hydroquinone were blended to the photosensitive resin, then shaped by the Asiga PRO2 3D printer. During this process, amorphous SiO_2 nanoparticles are the backbone of the preform, HEMA and POE are the monomer and dispersant, which allows the high amounts of silica nanoparticles dispersion owing to the formation of a solvation layer, without using further additives[7]. TEGDA, DPO and hydroquinone are the crosslinker, photoinitiator and inhibitor, respectively.

For the fiber core, 32.16% amorphous SiO_2 nanoparticles, 1.20 wt% GeO_2, 0.84 wt% TiO_2, 0.116 wt% $Bi_2(Al_2O_4)_3$, 0.014 wt% $ErCl_3$, 38.57 wt% HEMA, 19.90 wt% POE, 6.65 wt% TEGDA, 0.20 wt% DPO, 0.10 wt% hydroquinone and 0.25 wt% AIBN were mixed as the core resin. The combination of Bi and Er can provide an ultrabroad luminescence band covering the low loss telecommunication O-L band of silica fibers, thus the Bi and Er codoped active fibers hold potential to be used as an all-in-one broadband fiber amplifier to overcome the current internet communication traffic jam. However, the single doping of any of these ions would not have such a wide band luminescence[17,23]. The reason for using $Bi_2(Al_2O_4)_3$ instead of $BiCl_3$ was the early combination of bismuth and aluminum may help to improve the luminescence and stability of bismuth active center related aluminum. GeO_2 was used to increase the refractive index of the core region forming the waveguide structure. TiO_2 can form [TiO_4] tetrahedron and [TiO_6] octahedron structures in the fiber, enriching the fiber structure and thus being conducive to the broadband luminescence. It is worth noting that TiO_2 also increases the refractive index of the fiber core, so it is necessary to control the contents of TiO_2 and GeO_2 to avoid the refractive index difference between the fiber core and the cladding becoming too large. Al_2O_3 is designed to form bismuth active center related aluminum to provide luminescence at the central wavelength of 1100 nm and as the disperser to avoid the clustering of Er and Bi ions. The core material was poured into the channels of the printed cladding preform and cured at T = 60 ℃ and 90 ℃ for 2 hrs and 0.5 hrs, respectively[16]. The images of the preforms after 3D printing and after core materials filling are shown in Fig. 1a.

Measurements

The diffraction patterns were recorded using an X-ray diffractometer (D/MAX2550VB/PC, Rigaku Corporation, Japan) with CuKa irradiation over the angular range of $10° \le 2\theta \le 90°$. The EPMA images were measured by an electron probe microanalyzer (EPMA-1600, Shimadzu, Japan) with a wavelength-dispersive X-ray fluorescence spectroscopy (WDS). The refractive index and mode analysis were obtained from an optical fiber refractive index analyzer (SHR-1802, Shanghai University, China).

Transmission output patterns of kinds of BEDFs were

obtained using the setup shown in Fig. 1d, 532 nm LD was launched into the test fiber (~1 m) through × 40 microscope objective, then passed another microscope objective with the parameter of 8.18 mm/0.55 to image on the black screen. Loss spectrum of the single core BEDF was measured by cutback, shown in Fig. 4a. The white light was launched into the test fiber (~ 1 m) through a × 40 microscope objective, then chopped using a constant frequency, split by a monochromator and the optical signal converted to electrical signal through an InGaAs photo detector. Finally, the signal was amplified by a lock-in amplifier and recorded by a computer. The losses of three cores in the seven cores BEDF were also measured by cutback. The He-Ne laser was launched into each core one by one through the same microscope objective, and the output power recorded by a power meter. The emission spectra of the single core BEDF (~ 5 cm) were measured by the same monochromator system under excitation with 830 or 980 nm fiber laser respectively.

Acknowledgements

Authors are thankful for the two LIEF grants (LE0883038 and LE100100098) by Australian Research Council (ARC) to fund the National Fiber Facility at UNSW, Sydney. The National Science Foundation of China for grant (61775045). The Youth Program of National Natural Science Foundation of China for grant (62105078). The Youth Program of Natural Science Foundation of Shandong Province of China for grant (ZR2021QF009). Y. Chu and X. Fu also thank the support of the China Scholarship Council (CSC No. 201706680054 and 201708130199). Authors also thanks Dr C. Yan of Shanghai University for the measurements of refractive index and mode areas of BEDFs. JC acknowledge private funding of this work.

Author details

[1]Photonics and Optical Communications, School of Electrical Engineering and Telecommunications, University of New South Wales, Sydney, NSW 2052, Australia. [2]interdisciplinary Photonics Laboratories, University of Technology Sydney, NSW 2007 & University of Sydney, NSW 2006 Australia. [3]Key Laboratory of In-fiber Integrated Optics of Ministry of Education, College of Physics and Optoelectronic Engineering, Harbin Engineering University, Harbin 150001, China. [4]Fiber Optical Sensing Center for Excellence, Yantai Research Institute & Graduate School, Harbin Engineering University, Yantai 264000, China. [5]School of Information Science and Engineering, Key Laboratory for Special Fiber and Fiber Sensor of Hebei Province, Yanshan University, Qinhuangdao 066004, China

Author contributions

Y.C., J.Z. and G.D.P. proposed the idea and initiated the project. Y.C., X.F., Y.L. and G.D.P. fabricated optical fibers. Y.C., X.F., J.W. and Y.L. finished optical fiber characterization. Y.C., J.Z., Y.L., J.C., J.R. and G.D.P. analyzed the experimental data. Y.C. wrote the paper. JC provided predictions and explanations supported by the results in this paper. The manuscript was discussed and corrected by all authors.

Conflict of interest

The authors declare that they have no conflict of interest.

Received: 11 November 2021 Revised: 21 February 2022 Accepted: 23 February 2022
Accepted article preview online: 08 March 2022
Published online: 09 March 2022

References

1. Peng, G. D. et al. 3D silica lithography for future optical fiber fabrication. in Handbook of Optical Fibers (ed Peng, G. D.) (Singapore: Springer, 2019), 637-653.
2. Canning, J. & Cook, K. 3D printing, photonics and the IoT. Conference on Lasers and Electro-Optics/Pacific Rim 2018. Hong Kong, China: OSA, 2018, F1B.1.
3. Cook, K. et al. Air-structured optical fiber drawn from a 3D-printed preform. *Optics Letters* **40**, 3966-3969 (2015).
4. Cook, K. et al. Step-index optical fiber drawn from 3D printed preforms. *Optics Letters* **41**, 4554-4557 (2016).
5. Canning, J. et al. Drawing optical fibers from three-dimensional printers. *Optics Letters* **41**, 5551-5554 (2016).
6. Talataisong, W. et al. Novel method for manufacturing optical fiber: extrusion and drawing of microstructured polymer optical fibers from a 3D printer. *Optics Express* **26**, 32007-32013 (2018).
7. Kotz, F. et al. Three-dimensional printing of transparent fused silica glass. *Nature* **544**, 337-339 (2017).
8. Kotz, F. et al. Fabrication of arbitrary three-dimensional suspended hollow microstructures in transparent fused silica glass. *Nature Communications* **10**, 1439 (2019).
9. Nguyen, D. T. et al. 3D-printed transparent glass. *Advanced Materials* **29**, 1701181 (2017).
10. Destino, J. F. et al. 3D printed optical quality silica and Silica-Titania glasses from sol-gel feedstocks. *Advanced Materials Technologies* **3**, 1700323 (2018).
11. Zhang, D. et al. Highly efficient phosphor-glass composites by pressureless sintering. *Nature Communications* **11**, 2805 (2020).
12. Moore, D. G. et al. Three-dimensional printing of multicomponent glasses using phase-separating resins. *Nature Materials* **19**, 212-217 (2020).
13. Mader, M. et al. High-throughput injection molding of transparent fused silica glass. *Science* **372**, 182-186 (2021).
14. Rosales, A. L. C. et al. Optical fibers fabricated from 3D printed silica preforms. Proceedings of SPIE 11271, Laser 3D Manufacturing VII. San Francisco: SPIE, 2020, 112710U.
15. Zheng, B. L. et al. Fabrication of Yb-doped silica micro-structured optical fibers from UV-curable nano-composites and their application in temperature sensing. *Journal of Non-Crystalline Solids* **573**, 121129 (2021).
16. Chu, Y. et al. Silica optical fiber drawn from 3D printed preforms. *Optics Letters* **44**, 5358-5361 (2019).
17. Luo, Y. et al. Bismuth and erbium codoped optical fiber with ultrabroadband luminescence across O-, E-, S-, C-, and L-bands. *Optics Letters* **37**, 3447-3449 (2012).
18. Thipparapu, N. K. et al. 40 dB gain all fiber bismuth-doped amplifier operating in the O-band. *Optics Letters* **44**, 2248-2251 (2019).
19. Firstov, S. et al. Bismuth-doped optical fibers and fiber lasers for a spectral region of 1600-1800 nm. *Optics Letters* **39**, 6927-6930 (2014).
20. Chu, Y. et al. Topological engineering of photoluminescence properties of bismuth- or erbium-doped phosphosilicate glass of arbitrary P_2O_5 to SiO_2 Ratio. *Advanced Optical Materials* **6**, 1800024 (2018).
21. Chu, Y. et al. Fabrication and characterization of birefringent bismuth and erbium Co-doped photonic crystal fiber for broadband polarized near infrared emission. CLEO: Applications and Technology 2019. San Jose: OSA, 2019, JW2A.107.

22. Hao, J. et al. Effects of thermal treatment on photoluminescence properties of bismuth/erbium co-doped optical fibers. *Optical Fiber Technology* **46**, 141-146 (2018).
23. Dianov, E. M. Bismuth-doped optical fibers: a challenging active medium for near-IR lasers and optical amplifiers. *Light: Science & Applications* **1**, e12 (2012).
24. German, R. M. & Bose, A. Injection Molding of Metals and Ceramics. (Princeton, NJ, USA: Metal Powder Industries Federation, 1997).
25. Kotz, F. et al. Glassomerjprocessing fused silica glass like a polymer. *Advanced Materials* **30**, 1707100 (2018).
26. Miniscalco, W. J. Erbium-doped glasses for fiber amplifiers at 1500 nm. *Journal of Lightwave Technology* **9**, 234-250 (1991).
27. Canning, J. et al. Helical distributed feedback fiber Bragg gratings and rocking filters in a 3D printed preform-drawn fiber. *Optics Letters* **45**, 5444-5447 (2020).